Sinusoidal wavelength-scanning interferometric reflectometry

Osami Sasaki, Tomokazu Kuwahara, Ryohta Hara, and Takamasa Suzuki

We propose interferometric reflectometry in which a sinusoidal wavelength-scanning tunable laser diode is used to detect positions and profiles of multiple reflecting surfaces. An objective signal extracted from an interference signal contains modulation amplitude Z and phase α, which are related to the positions and profiles, respectively, of multiple reflecting surfaces. By using values of the objective signal at special times, we can produce an image intensity that shows where the reflecting surfaces exist. To obtain exact values of Z or values of α, we estimated the objective signal by using a conjugate gradient method. Experimental results show that a resolution of two-optical-path difference (OPD) in the image intensity is ~60 μm, and the final OPD precisions are 2 and 8 μm for two and three reflecting surfaces, respectively, for a wavelength-scanning width of 7 nm. Profiles of the front and rear surfaces of a silica glass plate with a thickness of 20 μm have been measured with a precision of ~10 nm.

OCIS codes: 120.3180, 110.4500, 120.6650.

1. Introduction

Reflectometers with a high depth resolution based on interferometry have been developed recently. There are two basic interferometric methods, optical coherence-domain reflectometry and optical frequency-domain reflectometry. In the former, the characteristics of the coherence function of a light source are utilized. A low-coherence source such as superluminescent diodes is used to achieve high depth resolution by scanning of a reference mirror. Optical coherence-domain reflectometry with a low-coherence interferometer is effectively applied to imaging of biological samples[1–4] and simultaneous measurement of the thickness and the refractive indices of transparent plates.[5–9] Moreover, a desirable coherence function is synthesized to eliminate the need to scan a reference mirror. The coherence function is synthesized through changes in the optical wavelength in the time domain[10] or by modification of a continuous spectrum in the space domain.[11] In optical frequency-domain interferometry the wavelength of a light source is scanned continuously, and the phase change of an interference signal that is due to the wavelength scanning produces high depth resolution without scanning of a reference mirror. The depth resolution is determined mainly by the wavelength-scanning width. In the case of wavelength scanning in the space domain,[12,13] a light source with a large spectral width is used, and interference intensities for the number of wavelengths are separated by a spectrometer along a one-dimensional direction. Because a spectrometer is used, an object must be scanned along the one-dimensional direction to yield the positions of multiple reflecting surfaces in three dimensions. Wavelength scanning in the time domain, however, does not require the scanning of an object. External-cavity tunable laser diodes (TLD's) are widely used to produce large wavelength-scanning widths.[14,15] When TLD's are used for linear wavelength scanning, any deviation from linearity in the scanning is a detrimental to achievement of high depth resolution. Reference 14 reports detection of the deviation from linearity by another interferometer to compensate for the deviation in the reflectometer.

In this paper we propose an optical frequency-domain reflectometry that uses sinusoidal wavelength scanning (SWS) in a TLD.[16] A mirror in the external cavity is vibrated rotationally by a galvanometer optical scanner to permit the wavelength to be scanned sinusoidally. Because the sinusoidal rotation is performed more precisely than the linear rotation, accurate SWS can be done.[17] This SWS

The authors are with the Faculty of Engineering, Niigata University, 8050 Ikarashi 2, Niigata-shi 950-2181, Japan. O. Sasaki's e-mail address is osami@eng.niigata-u.ac.jp.

Received 8 November 1999; revised manuscript received 20 April 2000.

0003-6935/00/220001-07$15.00/0

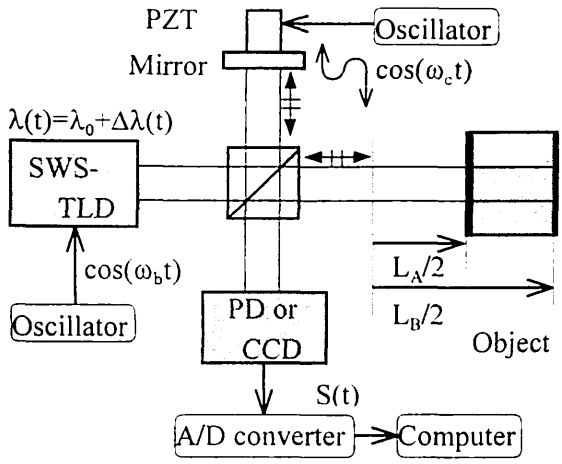

Fig. 1. Sinusoidal wavelength-scanning interferometric reflectometer: PZT, piezoelectric transducer; PD, photodiode; A/D, analog-to-digital.

leads to high depth resolution in SWS interferometric reflectometry. The interference signal contains a time-varying phase that is due to the SWS and a constant phase α. The amplitude of the time-varying phase is referred to as modulation amplitude Z. The positions and profiles of multiple reflecting surfaces are determined by values of Z and α, respectively. By manipulating values of the interference signal at the special times that we choose based on the position of a reflecting surface, we produce an image intensity that shows whether a reflecting surface exists at that position. After we obtain rough values of the positions of reflecting surfaces from the image intensity, we estimate the interference signal by using the rough values of the positions as initial values. The estimated signal provides exact values of the position and the surface profiles. Experimental results of position measurements with a photodiode reveal the basic characteristics of the SWS reflectometry. Profile measurements of the front and rear surfaces made with a two-dimensional CCD image sensor are also presented.

2. Principle

A schematic of the setup is shown in Fig. 1. The light source is a SWS TLD whose wavelength $\lambda(t)$ is expressed as $\lambda_0 + b\cos(\omega_b t)$. The reference wave is sinusoidally phase modulated with a vibrating mirror whose movement is expressed as $a\cos(\omega_c t + \theta)$.[18] An object has two surfaces, A and B, whose positions are expressed by optical path differences (OPD's) L_A and L_B, respectively. There are two object lights, which are reflected by surfaces A and B. A time-varying interference signal is given by

$$S(t) = A_A\cos[Z_c\cos(\omega_c t + \theta) + Z_A\cos(\omega_b t) + \alpha_A] + A_B\cos[Z_c\cos(\omega_c t + \theta) + Z_B\cos(\omega_b t) + \alpha_B], \quad (1)$$

where A_A and A_B are the amplitudes of the two interference signals caused by surfaces A and B, respectively, $Z_c = 4\pi a/\lambda_0$, and

$$Z_A = WL_A, \qquad Z_B = WL_B, \qquad W = 2\pi b/\lambda_0^2. \quad (2)$$

The Fourier transform of $S(t)$ is denoted $F(\omega)$, and the following conditions are satisfied:

$$\tilde{\mathcal{F}}\{\cos[Z_B\cos(\omega_b t) + \alpha_A]\} = 0,$$
$$\tilde{\mathcal{F}}\{\sin[Z_B\cos(\omega_b t) + \alpha_B]\} = 0,$$
$$|\omega| \geq \omega_c/2, \quad (3)$$

where $\tilde{\mathcal{F}}\{y\}$ is the Fourier transformation of y and $Z_A < Z_B$. We designate the frequency components of $F(\omega)$ that exist in the region of $\omega_c/2 < \omega < 3\omega_c/2$ by $F_1(\omega)$. Then we have

$$F_1(\omega + \omega_c) = -J_1(Z_c)\exp(j\theta)\tilde{\mathcal{F}}\{A_A\sin[Z_A\cos(\omega_b t) + \alpha_A] + A_B\sin[Z_B\cos(\omega_b t) + \alpha_B]\},$$
$$|\omega| \leq \omega_c/2, \quad (4)$$

where J_1 is a first-order Bessel function. The values of Z_c and θ that are related to phase modulation are measured by sinusoidal phase-modulating interferometry.[14] Taking the inverse Fourier transform of $-F_1(\omega + \omega_c)/J_1(Z_c)\exp(j\theta)$, we obtain

$$S_b(t) = A_A\sin[Z_A\cos(\omega_b t) + \alpha_A] + A_B\sin[Z_B\cos(\omega_b t) + \alpha_B]. \quad (5)$$

This signal is called an objective signal, and from it we obtain values of Z_A, Z_B, α_A, and α_B.

For simplicity we explain how to obtain a value of Z_A from an objective signal $S_b(t) = \sin[Z_A\cos(\omega_b t) + \alpha_A]$. We use special time t_i, which satisfies the equation

$$Z\cos(\omega_b t_i) = -Z + (\pi/2)(i - 1), \qquad i = 1, 2, 3, \ldots. \quad (6)$$

At that special time,

$$S_b(t_i) = \sin[\gamma + (\pi/2)(Z_A/Z)(i - 1)], \quad i = 1, 2, 3, \ldots, \quad (7)$$

where $\gamma = -Z_A + \alpha_A$.

At $Z_A/Z = 1, 3, 5, 7, \ldots$ we have the following equations:

$$S_b(t_1) = S_b(t_5) = \ldots = \sin\gamma,$$
$$S_b(t_2) = S_b(t_6) = \ldots = \begin{cases} -\cos\gamma & (Z_A/Z = 3, 7, \ldots) \\ \cos\gamma & (Z_A/Z = 1, 5, \ldots) \end{cases},$$
$$S_b(t_3) = S_b(t_7) = \ldots = -\sin\gamma,$$
$$S_b(t_4) = S_b(t_8) = \ldots = \begin{cases} \cos\gamma & (Z_A/Z = 3, 7, \ldots) \\ -\cos\gamma & (Z_A/Z = 1, 5, \ldots) \end{cases}. \quad (8)$$

At $Z_A/Z = 2$ we have the following equations:

$$S_b(t_1) = S_b(t_3) = S_b(t_5) = S_b(t_7) = \ldots = \sin\gamma,$$
$$S_b(t_2) = S_b(t_4) = S_b(t_6) = S_b(t_8) = \ldots = -\sin\gamma. \quad (9)$$

At $Z_A/Z = 4, 6, \ldots$ we have

$$S_b(t_i) = \sin\gamma, \qquad i = 1, 2, 3, \ldots. \tag{10}$$

When Z_A/Z is not an integer, $S_b(t_i)$ has different values for $i = 1, 2, 3, \ldots$. Considering the characteristics of $S_b(t_i)$, we define an image intensity as follows:

$$I(L) = (1/M)|S_b(t_1) - S_b(t_3) + S_b(t_5) - S_b(t_7) + \cdots|^2 + (1/M)|S_b(t_2) - S_b(t_4) + S_b(t_6) - S_b(t_8) + \cdots|^2, \tag{11}$$

where M is the maximum number of i. The image intensity has a maximum value at $Z_A/Z = 1, 3, 5, \ldots$ and is expected to be almost zero except in the region near $Z_A/Z = 1, 3, 5, \ldots$. We can obtain a rough value of Z_A from the peak position of the image intensity. When we consider multiple reflecting surfaces, we usually know the minimum value of Z for the surfaces. If there are two reflecting surfaces for which $S_b(t)$ is given by Eq. (5), we can also obtain rough values of Z_A and Z_B from the peaks of the image intensity when $Z_B/3 < Z_A < Z_B$.

Next we explain how to obtain exact values of Z_A, Z_B, α_A, and α_B. We estimate a signal

$$\hat{S}_b(t) = \hat{A}_A \sin[\hat{Z}_A \cos(\omega_b t) + \hat{\alpha}_A] + \hat{A}_B \sin[\hat{Z}_B \cos(\omega_b t) + \hat{\alpha}_B] \tag{12}$$

for the signal $S_b(t)$ that is actually detected. We define an objective function

$$B = \sum_{n=1}^{N} |S_b(t_n) - \hat{S}_b(t_n)|^2, \tag{13}$$

where t_n is a discrete time for the signals. We search by the conjugate gradient method for values of the variables in Eq. (12) that minimize B. The rough values of Z_A and Z_B obtained from the image intensity are used as the initial values for the estimation.

The positions of surfaces A and B are given by $L_A = \hat{Z}_A/W$ and $L_B = \hat{Z}_B/W$, respectively, in the OPD. The front surface profile r_A and the rear surface profile r_B are given by

$$r_A = (\lambda_0/4\pi)\alpha_A, \qquad r_B = (\lambda_0/4\pi n_R)[(n_R - 1)\alpha_A + \alpha_B], \tag{14}$$

where the refractive index n_R of the object is constant in the object. Thus we can obtain the positions and profiles of multiple reflecting surfaces from values of Z and α, respectively.

3. Experiments

A. Experimental Setup

Experiments were carried out with the setup shown in Fig. 1. Figure 2 shows a configuration of the SWS TLD. The output beam from a laser diode (LD) is collimated by lens L and is incident upon diffraction grating G. The first-order reflection from the grating is reflected back into the laser diode by mirror M. The zero-order reflection from the grating is the output beam of the SWS TLD. We scanned the wavelength by rotating the mirror sinusoidally with an angular frequency ω_b. We used a laser diode whose central wavelength λ_0 and output power were 783 nm and 50 mW, respectively. A 1200-line/mm holographic grating was used with incident angles φ_i of 75°. The mirror was vibrated rotationally about a 5° angle φ_d by a galvanometer optical scanner.

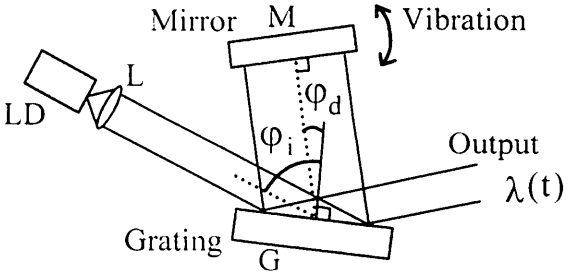

Fig. 2. Configuration of the SWS TLD.

B. Position Measurements

We detected an interference signal $S(t)$ for one point of an object with a photodiode. The frequencies of $\omega_b/2\pi$ and $\omega_c/2\pi$ were 30 and 1920 Hz, respectively. The sampling frequency for the interference signals was $16\times\ \omega_c/2\pi$, and the signals were processed with a personal computer.

First we tried to measure the thickness of a vinyl sheet with two surfaces, A and B, as shown in Fig. 1. Figure 3 shows objective signal $S_b(t)$ extracted from the detected interference signal. Figure 4 shows image intensity $I(z)$ obtained from objective signal $S_b(t)$ of Fig. 3. It can be seen from image intensity $I(z)$ that there are two surfaces, at $Z_A = 9$ rad and $Z_B = 14$ rad. These rough values became the initial values for estimating signal $\hat{S}_b(t)$ by the conjugate gradient method. Figures 5 and 6 show that the value of objective function B approached zero and the value of $\hat{Z}_A$ changed from 9 to 9.21 as the estimation was iterated. Estimated signal $\hat{S}_b(t)$ is shown in Fig. 7 and is almost equal to objective signal $S_b(t)$ of Fig. 3.

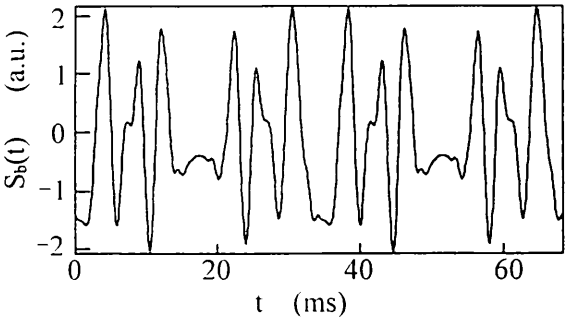

Fig. 3. Objective signal $S_b(t)$ extracted from the interference signal detected for a vinyl sheet with two surfaces.

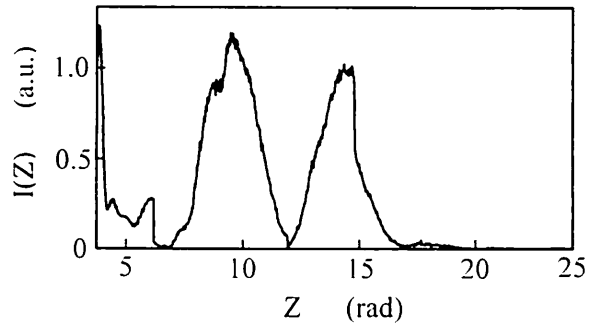

Fig. 4. Image intensity $I(z)$ obtained from objective signal $S_b(t)$ of Fig. 3.

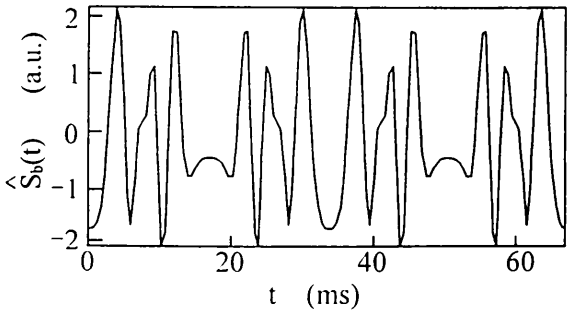

Fig. 7. Estimated signal $\hat{S}_b(t)$ almost equal to objective signal $S_b(t)$ of Fig. 3.

The estimated results were $\hat{Z}_A = 9.21$ rad and $\hat{Z}_B = 14.61$ rad. Now we have to determine a value of $W = 2\pi b/\lambda_0^2$. We measured values of $\hat{Z}$ for surfaces A and B every time the object was displaced, which increased L_A and L_B by 10 μm. We show the measured result in Fig. 8, where change ΔL in the OPD reached 90 μm. We determined (Fig. 8) that W was equal to 3.46×10^{-2} rad/μm. Because $\lambda_0 = 783$ nm, the wavelength-scanning width $2b$ was 6.8 nm. Using the relation $Z = WL$, we obtained $L_A = 266$ μm and $L_B = 422$ μm and a thickness $d = (L_A - L_B)/2n_R = 54.9$ μm, where the refractive index n_R of the vinyl sheet was 1.42. To determine the repeatability of the measurement, we measured the values of $\hat{Z}$ for surfaces A and B at intervals of 10 s, as shown in Fig. 9. It became clear (Fig. 9) that the measurement error of Z was 0.07 rad and the corresponding error of L was 2 μm. Therefore we could measure the thickness of the vinyl sheet with a precision of 0.7 μm. We expected from Fig. 4 that two reflecting surfaces could be distinguished for image intensity $I(z)$ if difference in Z between the two surfaces were more than 2 rad. This value corresponds to an ~60-μm OPD, which is called two-OPD resolution. We achieved a

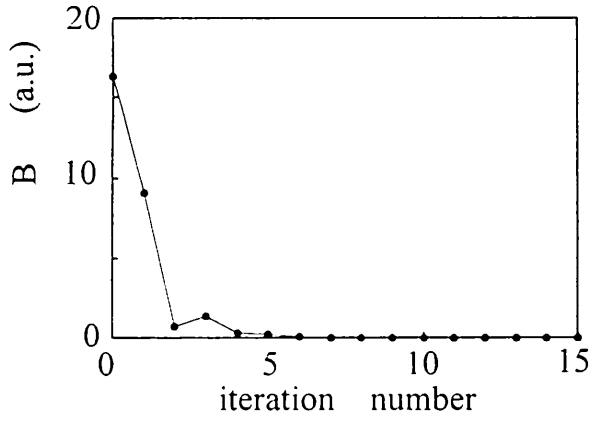

Fig. 5. Values of objective function B versus number of iterations.

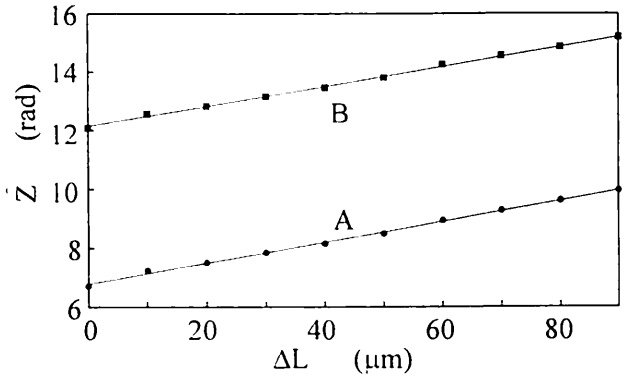

Fig. 8. Values of $\hat{Z}$ for the two surfaces. A and B, measured every time the object was displaced such that the change ΔL in the OPD increased by 10 μm.

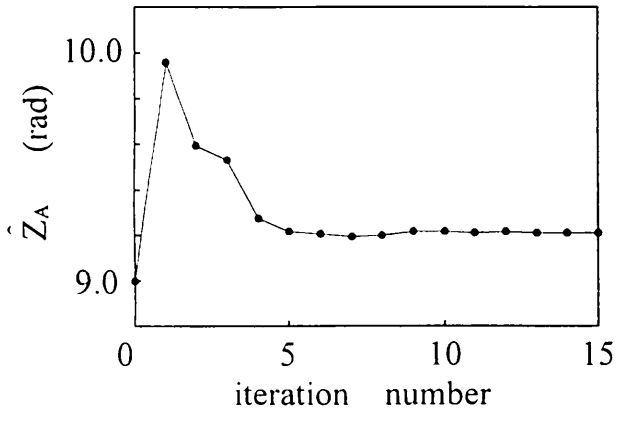

Fig. 6. Value of $\hat{Z}_A$ versus number of iterations.

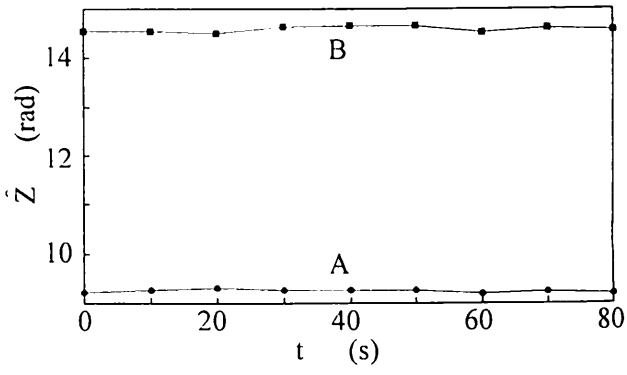

Fig. 9. Values of $\hat{Z}$ for two surfaces. A and B, measured at intervals of 10 s.

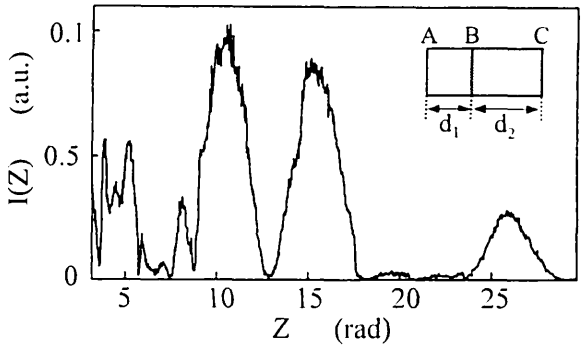

Fig. 10. Image intensity $I(z)$ obtained for the three surfaces, A, B, and C, of a vinyl sheet.

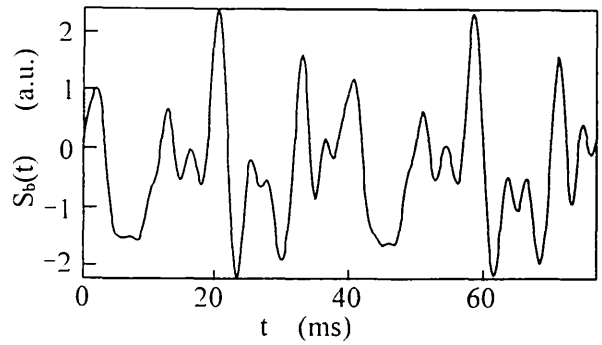

Fig. 12. Objective signal $S_b(t)$ extracted from the interference signal detected for a silica glass plate with thickness of 20 μm.

two-OPD resolution of 60 μm and an OPD precision of 2 μm when we measured two positions.

Next we measured the positions of three surfaces, A, B, and C of two vinyl sheets in contact with each other and with thicknesses A–B = d_1 and B–C = d_2, as shown in Fig. 10. Figure 10 shows the image intensity $I(z)$ from which we obtained Z_A = 11 rad, Z_B = 16 rad, and Z_C = 27 rad. Estimated signal $\hat{S}_b(t)$ was almost equal to objective signal $S_b(t)$, and we obtained $\hat{Z}_A$ = 10.04 rad, $\hat{Z}_B$ = 15.91 rad, and $\hat{Z}_C$ = 26.74 rad. From the relation $Z = WL$, we obtained the measurement results L_A = 290 μm, L_B = 460 μm, and L_C = 773 μm, that is, d_1 = 60 μm and d_2 = 110 μm. To determine the repeatability of the measurement we repeated the measurement of $\hat{Z}$ for the three surfaces at intervals of 10 s, as shown in Fig. 11. From the result, the measurement error of Z was 0.28 rad and the corresponding error of L was 8 μm. In the measurement of three positions compared with two positions the two-OPD resolution does not change but the OPD precision deteriorates. It appears that noise contained in objective signal $S_b(t)$ has a bad effect on the estimation of $\hat{S}_b(t)$ because of the larger number of variables for three-position measurements.

C. Surface-Profile Measurements

We tried to measure the front and rear surface profiles of a silica glass plate with a thickness of 20 μm. We used 8 × 16 elements of a two-dimensional CCD image sensor to obtain interference signals in a region of 0.68 mm × 1.04 mm. The measurements were made at intervals of 85 and 65 μm along the x and y axes, respectively. The frequencies of $\omega_b/2\pi$ and $\omega_c/2\pi$ were 26 and 832 Hz, respectively. The output of the CCD image sensor at one measuring point was sampled with a frequency of $f_s = 8 \times \omega_c/2\pi$. Because the output was an integration value of the interference signal given by Eq. (1) over a period of $1/f_s$, the output was converted into an interference signal as described in Ref. 19.

Figure 12 shows objective signal $S_b(t)$ extracted from the detected interference signal. Figure 13 shows image intensity $I(z)$ obtained from objective signal $S_b(t)$ of Fig. 12. One can see from Fig. 13 that there are two surfaces near Z_A = 8 rad and Z_B = 10 rad. Estimated signal $\hat{S}_b(t)$ was almost equal to objective signal $S_b(t)$ of Fig. 12. Figure 14 shows profiles of the front and rear surfaces calculated from the estimated values of α_A and α_B with Eqs. (14). We made the same measurement after 10 min to determine the repeatability of the measurement. The root-mean-square value of the difference between the two measured profiles for the front and rear surfaces was ~10 nm. We expected that the estimated values of Z_A and Z_B would be almost constant in the measuring region, but their values fluctuated with a width of ~1.5 rad. This experimental result indicates that an exact estimation of modulation amplitude Z is difficult when objective signal $S_b(t)$ contains

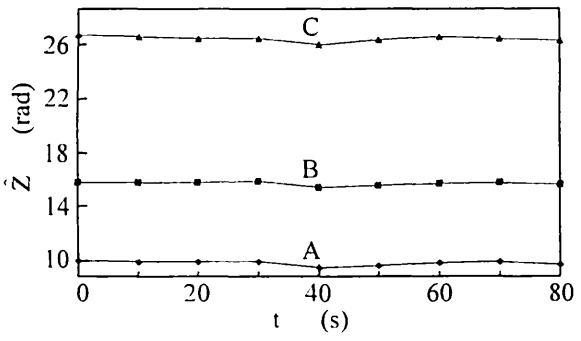

Fig. 11. Values of $\hat{Z}$ for the three surfaces, A, B, and C, measured at intervals of 10 s.

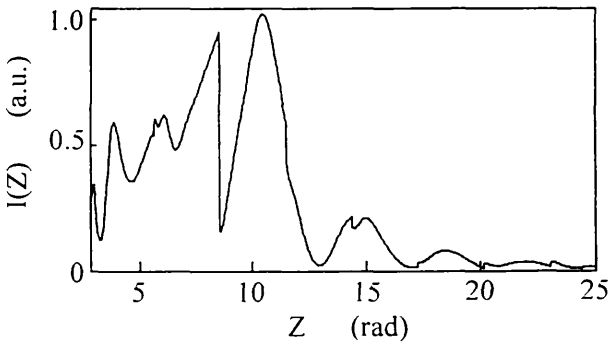

Fig. 13. Image intensity $I(z)$ obtained from objective signal $S_b(t)$ of Fig. 12.

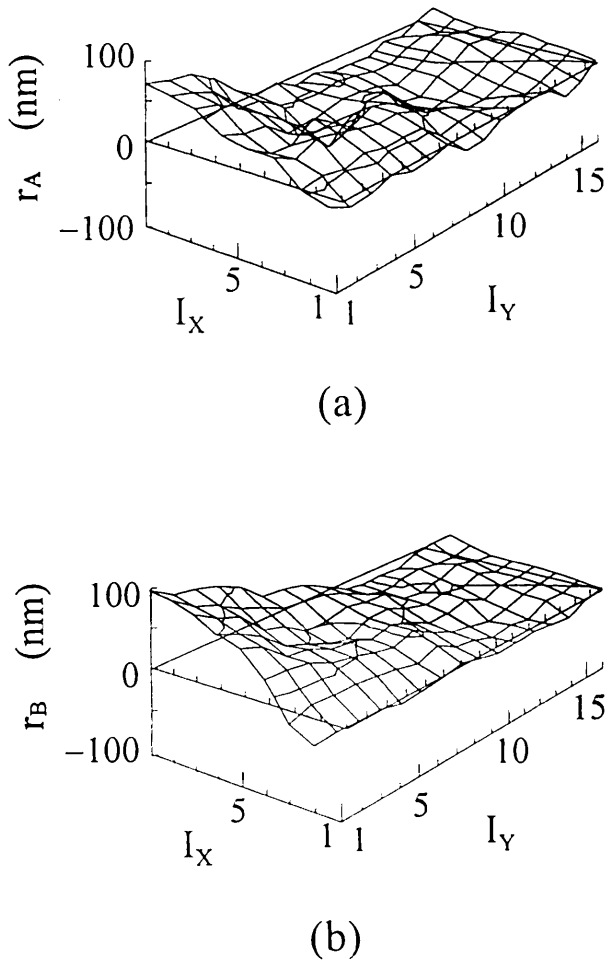

Fig. 14. Measured profiles of (a) the front surface and (b) the rear surface of the silica glass plate.

a large amount of noise. Computer simulations showed that the estimation of phase α was not influenced so much by noise as was that of Z. When the estimated values of Z deviated from the correct values within ± 2 rad, the estimation error of phase α was less than 0.1 rad. This computer simulation result supports our conclusion that the front and rear surfaces can be measured with a precision of ~ 10 nm.

4. Conclusions

We have proposed an interferometric reflectometry in which we used a sinusoidal wavelength-scanning tunable laser diode to detect the positions and profiles of multiple reflecting surfaces. We also sinusoidally phase modulated the reference wave with a vibrating mirror to extract objective signal $S_b(t)$ from the interference signal. Objective signal $S_b(t)$ contains modulation amplitude Z and phase α, which are related to the positions and profiles of the multiple reflecting surfaces, respectively. By using the values of $S_b(t_i)$ at a special time t_i that depends on the value of $Z = WL$, we can produce image intensity $I(Z)$. The image intensity has a large value at Z if a reflecting surface exists at the positions of L in the optical path difference. From $I(Z)$ we obtain rough values of Z that correspond to the positions of the multiple reflecting surfaces, which we use as initial values for estimating the objective signal to obtain exact values of Z or values of α.

In position measurements with a photodiode, the two-OPD resolution in the image intensity was ~ 60 μm when the wavelength-scanning width was 6.8 nm. The OPD precision was 2 μm for a measurement of two positions, and a 55-μm thickness of a vinyl sheet was measured with a precision of 0.7 μm. The OPD precision was 8 μm for a measurement of three positions. In surface-profile measurements with a two-dimensional CCD image sensor, the front and rear surfaces of a silica glass plate with a thickness of 20 μm were measured with a precision of ~ 10 nm. Although the noises contained in the objective signal influenced the estimation of Z, they had less influence on the estimation of α.

References

1. D. Huang, E. A. Swanson, C. P. Lin, J. S. Schuman, W. G. Stinson, W. Chang, M. R. Hee, T. Flotte, K. Gregory, C. A. Puliafito, and J. G. Fujimoto, "Optical coherence tomography," Science **254,** 1178–1181 (1991).
2. A. F. Fercher, C. K. Hitzenberger, W. Drexler, G. Kamp, and H. Sattmann, "*In vivo* optical coherence tomography," Am. J. Ophthalmol. **116,** 113–114 (1993).
3. J. A. Izatt, M. R. Hee, G. M. Owen, E. A. Swanston, and J. G. Fujimoto, "Optical coherence microscopy in scattering media," Opt. Lett. **19,** 590–592 (1994).
4. M. J. Yadlowsky, J. M. Schmitt, and R. F. Bonner, "Multiple scattering in optical coherence microscopy," Appl. Opt. **34,** 5699–5707 (1995).
5. A. F. Fercher, K. Mengedoht, and W. Werner, "Eye length measurement by interferometry with partially coherent light," Opt. Lett. **13,** 186–188 (1988).
6. D. Huang, J. Wang, C. P. Lin, C. A. Puliafito, and J. G. Fujimoto, "Micron-resolution ranging of cornea anterior chamber by optical reflectometry," Lasers Surg. Med. **11,** 419–425 (1991).
7. G. J. Tearney, M. E. Brezinski, J. F. Southern, B. E. Bouma, M. R. Hee, and J. G. Fujimoto, "Determination of the refractive index of highly scattering human tissue by optical coherence tomography," Opt. Lett. **20,** 2258–2260 (1995).
8. T. Fukano and I. Yamaguchi, "Simultaneous measurement of thickness and refractive indices of multiple layers by a low-coherence confocal interference microscope," Opt. Lett. **21,** 1942–1944 (1996).
9. M. Haruna, M. Ohmi, T. Mitsuyama, H. Tajiri, H. Maruyama, and M. Hashimoto, "Simultaneous measurement of the phase and group indices and the thickness of transparent plates by low-coherence interferometry," Opt. Lett. **23,** 996–968 (1998).
10. Z. He, N. Mukohzaka, and K. Hotate, "Selective image extraction by synthesis of the coherence function using two-dimensional optical lock-in amplifier with microchannel spatial light modulator," IEEE Photon. Technol. Lett. **9,** 514–516 (1997).
11. Y. Teramura, K. Suzuki, M. Suzuki, and F. Kannari, "Low-coherence interferometry with synthesis of coherence function," Appl. Opt. **38,** 5974–5980 (1999).
12. A. F. Fercher, C. K. Hitzenberger, G. Kamp, and S. Y. El-Zaiat, "Measurement of intraocular distances by backscattering spectral interferometry," Opt. Commun. **117,** 43–48 (1995).

13. T. Funaba, N. Tanno, and H. Ito, "Multimode-laser reflectometer with a multichannel wavelength detector and its application," Appl. Opt. **36,** 8919–8928 (1997).
14. F. Lexer, C. K. Hitzenberger, A. F. Fercher, and M. Kulhavy, "Wavelength-tuning interferometry of intraocular distances," Appl. Opt. **36,** 6548–6553 (1997).
15. T. Yoshimura, H. Hiratuka, E. Kido, and K. Yamada, "Optical coherence tomography in scattering media using a continuous wave tunable laser diode," in *Laser Interferometry IX: Applications*, R. J. Pryputniewicz, G. M. Brown, and W. P. O. Jupter, eds., Proc. SPIE **3479,** 207–214 (1998).
16. O. Sasaki, T. Kuwahara, R. Hara, and T. Suzuki, "Sinusoidal wavelength-scanning interferometeric reflectometry," in *Optical Engineering for Sensing and Nanotechnology*, I. Yamaguchi, ed., Proc. SPIE **3740,** 618–621 (1999).
17. O. Sasaki, K. Tsuji, S. Sato, T. Kuwahara, and T. Suzuki, "Sinusoidal wavelength-scanning interferometers," in *Laser Interferometry IX: Techniques and Analysis*, M. Kujawinska, G. M. Brown, and M. Takeda, eds., Proc. SPIE **3478,** 37–44 (1998).
18. O. Sasaki, T. Yoshida, and T. Suzuki, "Double sinusoidal phase-modulating laser diode interferometer for distance measurement," Appl. Opt. **30,** 3617–3621 (1991).
19. O. Sasaki and H. Okazaki, "Detection of time-varying intensity distribution with CCD image sensors," Appl. Opt. **24,** 2124–2126 (1986).